Atmospheric Environment 85 (2014) 73–82

Contents lists available at ScienceDirect

Atmospheric Environment

journal homepage: www.elsevier.com/locate/atmosenv

Estimation of direct emissions and atmospheric processing of reactive mercury using inverse modeling

Benjamin de Foy [a,b,*], Jongbae Heo [c], James J. Schauer [c]

[a] Department of Earth and Atmospheric Sciences, Saint Louis University, USA
[b] Earth and Life Institute, Université catholique de Louvain, Belgium
[c] Civil & Environmental Engineering, University of Wisconsin–Madison, USA

HIGHLIGHTS

- 50–70% of reactive mercury in Milwaukee is from direct emissions.
- Direct emissions are much higher than in most current chemical transport simulations.
- 15% of reactive gaseous mercury is estimated to be due to free tropospheric transport.
- Ozone oxidation of GEM is better represented in models than OH and Br oxidation.

GRAPHICAL ABSTRACT

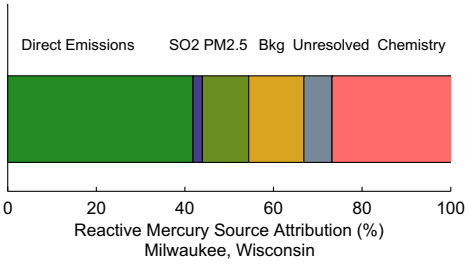

ARTICLE INFO

Article history:
Received 15 September 2013
Received in revised form
20 November 2013
Accepted 28 November 2013

Keywords:
Mercury
Reactive mercury
Emissions inventory
Inverse modeling
Mercury oxidation

ABSTRACT

There are large uncertainties in the estimation of sources of reactive mercury in current photochemical models, with many models suggesting that three quarters or more of reactive mercury in the atmosphere is due to secondary oxidation of the gaseous elemental mercury present in the global background. An inverse model is used to estimate the sources of mercury at an urban site in Wisconsin based on a year long time series of hourly measurements. The model combines high resolution backtrajectories simulated with WRF and WRF-FLEXPART, forward simulations of passive tracers using a transport model (CAMx), hourly time series of atmospheric pollutant concentrations and time series from a chemical box model for oxidation of elemental mercury by ozone, the hydroxyl radical and bromine. The hybrid formulation provides an estimate of the mercury concentrations on a polar grid surrounding the site along with emission scaling factors for emissions from forest fires and lake surfaces. In addition, the model estimates the impact of oxidation of gaseous elemental mercury from the three pathways. The inverse model identified direct emissions of reactive mercury, defined as the sum of reactive gaseous mercury and particle-bound mercury, that are associated with regional sources and with forest fires. The results suggest that oxidation by ozone is adequately characterized in existing chemical mechanisms, but that oxidation by the hydroxyl radical and by bromine may be underestimated. The results suggest that between 50 and 70 percent of the reactive mercury at the measurement site is due to direct emissions and hence suggest the importance of developing emission inventories for reactive mercury species.

1. Introduction

Mercury is a powerful neurotoxin that is globally present in the atmosphere (Mergler et al., 2007). Despite its relevance to human and ecosystem health, significant uncertainties remain in its

* Corresponding author. Department of Earth and Atmospheric Sciences, Saint Louis University, USA. Tel.: +1 314 977 3122.
E-mail address: bdefoy@slu.edu (B. de Foy).

1352-2310/$ – see front matter © 2013 Elsevier Ltd. All rights reserved.
http://dx.doi.org/10.1016/j.atmosenv.2013.11.070

emissions inventories and its atmospheric reactions (Gustin and Jaffe, 2010; Lindberg et al., 2007). Common measurements distinguish between mercury in three forms: Gaseous Elemental Mercury (GEM), Reactive Gaseous Mercury (RGM), and Particle-bound mercury (PHg), with Reactive Mercury (RHg) being the sum of RGM and PHg. Although most of the mercury in the atmosphere is in the form of GEM, deposition of RGM and PHg is much faster (Zhang et al., 2012a). The deposited mercury reacts to form methylmercury which leads to bio-accumulation and adverse health effects.

There are significant discrepancies between simulated and measured levels of RHg (Holloway et al., 2012; Bullock et al., 2008, 2009), which are thought to be mainly due to limitations in our understanding of the chemical mechanisms (Sillman et al., 2007; Lin et al., 2006, 2007), to uncertainties in the parameterization of deposition (Baker and Bash, 2012) and to measurement uncertainties (see Section 2.2). Both aqueous (Subir et al., 2011) and heterogeneous (Subir et al., 2012; Rutter et al., 2012) reactions play a significant role in these uncertainties leading to the potential for compensating errors (Lin et al., 2006). The lifetime of GEM was estimated to be approximately 1 year (Lindberg et al., 2007), but Holmes et al. (2010) suggests that it could be as low as 6 months due to oxidation by bromine.

RGM has been found to correlate with ozone, suggesting secondary formation, as well as with sulfur dioxide, suggesting direct emissions (Lindberg and Stratton, 1998). A combination of measurements and simulations suggest the importance of RGM transport events in the free troposphere (Huang and Gustin, 2012). In addition to the uncertainty about the oxidation of mercury, there is uncertainty about the reduction of RGM to GEM, either specifically in power plant plumes (Zhang et al., 2012b) or in the general atmosphere (Pongprueksa et al., 2008) which can introduce excessive simulated RHg if in-stack emission factors are used and near field chemical transformations are not addressed (Lohman et al., 2006). In current models, most of the RGM is due to photochemical oxidation of GEM. This leads to very high estimates of the impact of the global background on local deposition (Holloway et al., 2012; Zhang et al., 2012b; Lin et al., 2012; Selin and Jacob, 2008; Seigneur et al., 2004).

This study uses an inverse model to estimate direct emissions and chemical formation of reactive mercury based on a year-long time series of hourly speciated mercury concentrations. As an alternative to the use of Eulerian models using mercury chemical mechanisms, we develop a method that uses backtrajectories, forward simulations of passive tracers, surface concentrations of tracer species and simulations of RGM formation from GEM oxidation from a chemical box model. By developing an approach that does not rely on a full chemical simulation, we seek to provide constraints on mercury sources and reactions that are complementary to existing studies. The inverse method is based on de Foy et al. (2012b) who used it to estimate GEM emissions from forest fires, lakes, regional and local sources. We have expanded the method in order to be able to estimate emissions and chemical formation of reactive mercury.

2. Methods

2.1. Inverse model

The inverse model estimates emissions due to sources surrounding the receptor site by using backtrajectories of passive tracers that have been mapped onto a polar grid. This is combined with forward Eulerian simulations of passive tracers from selected source groups, in a manner similar to the two-step method (Rigby et al., 2011; Roedenbeck et al., 2009). The inverse model produces emission scaling factors for each source term included in the forward transport simulations. When multiplying the a priori emissions by the emission scaling factor we obtain the a posteriori emissions estimate. Fig. 1 shows a flowchart of the inverse model process.

The inversion generates an estimate of "gridded emissions" on a grid that stretches out 1000 km from the receptor site. These gridded emissions are a posteriori estimates based on a priori emissions set to zero. They do not include emissions that are better

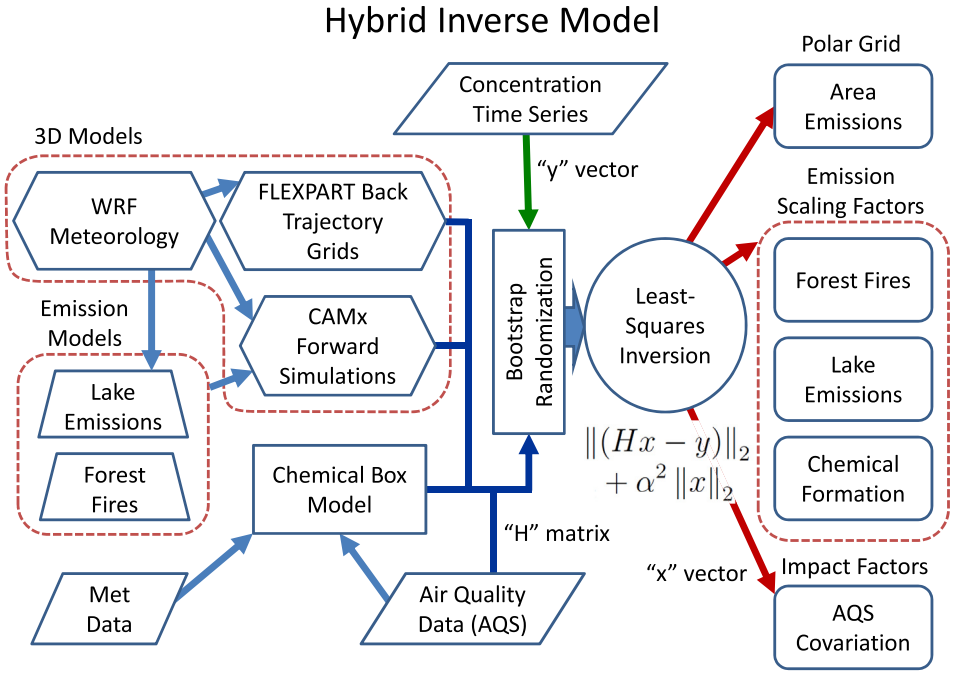

Fig. 1. Flowchart of the inverse model showing the combination of inputs from backtrajectories, forward simulations, chemical box model and air quality data (AQS) into the matrix *H*. The output vector *x* of the inversion is a hybrid containing area emissions, emission scaling factors for forest fires, lake emissions and chemical formation as well as impact factors for air quality data.

accounted for by another part of the inversion, for example the forest fires and the lake surface emissions, but do include an estimate of remaining area and point sources for each grid cell in the polar grid.

The inverse model also includes measured species concentrations for SO_2 and $PM_{2.5}$. SO_2 concentrations can serve as a proxy for large regional point sources. Therefore, the amount of mercury that co-varies with SO_2 can be interpreted as an estimate of the mercury from these sources present as GEM, RGM or PHg. In a similar fashion, the amount of mercury that co-varies with $PM_{2.5}$ represents an estimate of the GEM, RGM or PHg associated with general aerosol loadings. Finally, the inverse model includes simulations from a chemical box model, as will be described below.

By limiting the input of the model to passive tracers and individual time series, we can use a least-squares simplification developed in de Foy et al. (2012b) to the Bayesian formulation used in Stohl et al. (2009). This hybrid least-squares method derives an estimate of the emissions vector x that minimizes the cost function J given by the sum of the observation cost function and the emissions cost function:

$$J = \|(Hx - y)\|_2 + \alpha^2 \|x\|_2 \quad (1)$$

Where y is the vector of measurements, H is the sensitivity matrix that converts emissions parameters x into simulated concentrations, and α is the regularization parameter that balances the two parts of the cost function. This method was shown to be equivalent to a Bayesian derivation when diagonal error covariance matrices are used (de Foy et al., 2012b; Wunsch, 2006; Aster et al., 2012). The regularization parameter replaces the uncertainty estimates of the measurements and the emissions vector that are required by the Bayesian method, and is obtained empirically as described below.

Both H and x are hybrid: they contain terms that represent the concentrations associated with: 1. gridded emissions, 2. forward simulations of passive tracers, 3. surface concentration measurements, 4. simulated RHg time series from a chemical box model and 5. background terms. There is a column in H for each grid cell in the gridded emissions. These represent the concentration at the receptor site due to unit emissions from that cell. The corresponding entry in x is an estimate of the emissions from that cell. In this work we use a zero prior for the gridded emissions. There are additional columns in H containing the concentrations simulated by CAMx for specific source groups. For these cases, the corresponding entry in x is a scaling factor on the prior source emissions used as input to CAMx. The US Environmental Protection Agency's Air Quality System (AQS) time series and the chemical box model time series are normalized and included in H. The corresponding scaling factor gives an estimate of the amount of mercury that is associated with these processes. The final column is a unit vector with corresponding x equivalent to the background level of the concentrations.

The system of equations can be solved with a single step of least-squares using:

$$J = \|s \cdot (H'' x - y'')\|_2 \quad (2)$$

Where H'' and y'' are augmented versions of H and y to include both parts of the cost function, and s contains scaling factors on the parts of the cost function: these are taken to be unit values for the observation cost function and contain the regularization parameter α for the emissions cost function. Boundaries are applied to the vector x during the least-squares solutions to prevent nonphysical negative emissions. An Iteratively Reweighted Least-Squares (IRLS) scheme is used to reduce the sensitivity of the method to outliers in the data: after solving for x, observation times that have a residual larger than 3 times the standard deviation of the residual values are removed from the analysis. This is performed iteratively to converge on a stable set of values.

In a Bayesian framework, uncertainty estimates are required to obtain the error covariance matrices on the two parts of the cost function. In the least-squares framework, these are not needed because an optimization routine can be used to determine the values of the regularization parameters in the vector s that minimize the total error following (Henze et al., 2009). These are determined sequentially for the gridded emissions, for the forest fire and lake emission impacts, for the free tropospheric term, for the air quality concentration time series, for the chemical box model time series and for the background value. The regularization parameter for the gridded emissions is scaled by the cell area to account for the increase in uncertainty with increasing distance from the measurement site.

The inverse model was performed for GEM, RGM, PHg and RHg. As the inversion is solved by a least-squares method it takes less than a minute to run. We therefore use block bootstrapping to estimate the uncertainty on the results due to the selection of input data and the errors in the transport models. There are 299 days with valid data. 100 inversions were performed with 299 days of data selected at random with replacement from the dataset. The standard deviation of the output vector x gives an estimate of the uncertainty in the inversion due to both measurement error and transport modeling errors, see Section 3 for further discussion.

2.2. Measurements

Speciated mercury measurements were made at an urban site from June 28, 2004 to May 12, 2005 located at 2114 E. Kenwood Blvd, Milwaukee, WI (MKE, 43.07°N, 87.88°W) which is 5 km north of the downtown area and about 1 km from Lake Michigan. GEM, RGM and PHg were measured in real time with an in situ ambient mercury analyzer (Tekran, Inc., Toronto, Ontario, Canada) and are described in detail in (Rutter et al., 2008; Manolopoulos et al., 2007a). One-hour average concentrations were measured on alternate hours for the duration of the experiment.

The mercury measurements from the Tekran instrument are operationally defined and have been found to be reproducible, see for example Manolopoulos et al. (2007b). However, results from the Reno Atmospheric Intercomparison eXperiment (RAMIX, Gustin et al., 2013) suggest that they may underestimate concentrations of RHg by up to a factor of 2 or 3. This would mean that emissions estimates based on Tekran measurements would be significantly biased low.

Concurrent hourly air quality measurements of O_3, SO_2 and $PM_{2.5}$ were made by the Wisconsin Department of Natural Resources (WIDNR) at their headquarters 3 km southwest of the urban location. These were retrieved from the AQS database.

Hourly meteorological observations were obtained for General Mitchell International Airport (KMKE), 10 miles south of the measurement site, from the Integrated Surface Hourly Data available from the National Climatic Data Center.

2.3. Numerical simulations

The numerical simulations of meteorology and wind transport used in this study were described in detail in (de Foy et al., 2012b,a) and can be summarized as follows: meteorological simulations were performed with the Weather Research and Forecast (WRF) model (Skamarock et al., 2005), and were initialized with the North American Regional Reanalysis (Mesinger et al., 2006). For the urban site, the model was run on 3 domains with 27, 9 and 3 km horizontal resolution and 40 vertical levels using version 3.3.1, see Fig. 2

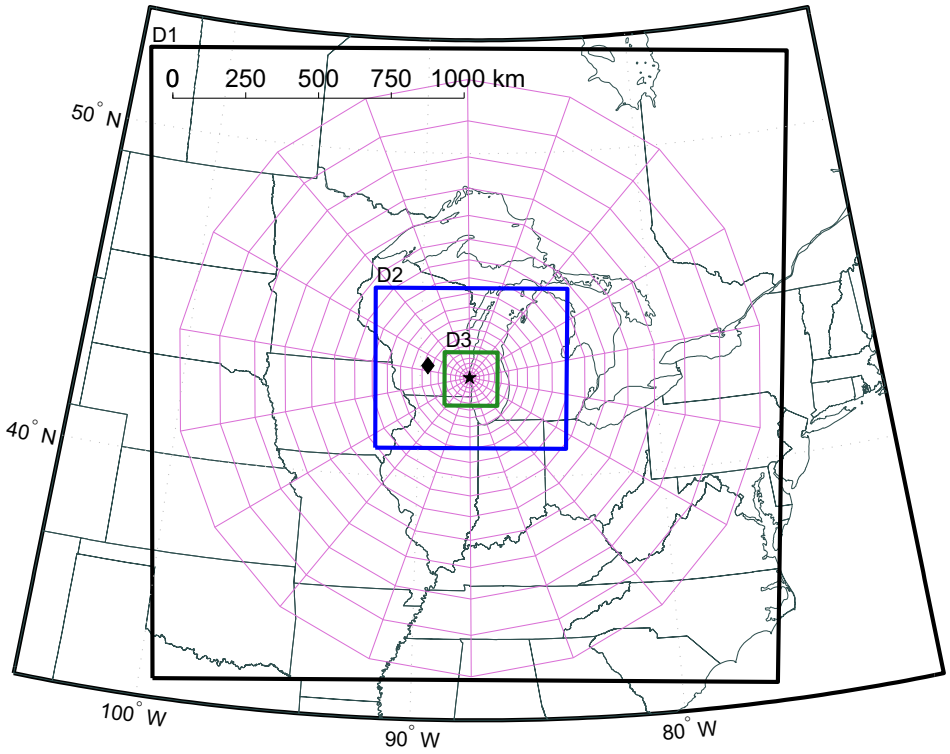

Fig. 2. Map showing the 3 WRF domains, the measurement site (star) and the rural site (diamond). Particle backtrajectories were mapped onto the polar grid for the estimation of gridded emissions.

for a map of the domains. The model was run with two-way nesting, with the Yonsei University (YSU) boundary layer scheme, the Kain–Fritsch convective parameterization, the NOAH land surface scheme, the WSM 3-class simple ice microphysics scheme, the Goddard shortwave scheme and the Rapid Radiation Transfer Model longwave scheme. Individual simulations were performed lasting 162 h, of which the first 42 h were considered spin-up time and the remaining 5 days were used for analysis.

Particle backtrajectories were calculated with FLEXPART (Stohl et al., 2005), using WRF-FLEXPART (Fast and Easter, 2006) for 6 days duration starting every hour of the campaign. 1000 particles were released per hour between 0 and 50 m above the ground and were allowed to disperse in three dimensions using the WRF mixing heights and surface friction velocity. The particle positions were converted to polar grids to provide a Residence Time Analysis (RTA, Ashbaugh et al., 1985). This represents the amount of time that an air mass has spent in different grid cells before arriving at the measurement location and can be rescaled to yield the impact that a source in each grid cell would have at the receptor site (Seibert and Frank, 2004).

The Comprehensive Air-quality Model with eXtensions (CAMx v5.40, ENVIRON (2011)), an Eulerian 3D grid model, was used to simulate the passive transport of GEM for emissions from known sources as input to the inverse model. This study is focused on estimating source contributions from individual factors and therefore does not use the mercury chemical module in CAMx. CAMx was run with domains 1 and 2 of the WRF simulations and provided hourly GEM concentrations at the receptor sites. The GEM time series were included in the inverse model of the reactive forms of mercury (RGM, PHg, RHg) in order to estimate the emissions of these forms as a fraction of the GEM emissions estimates. The sources include the lake surface, forest fires and the free troposphere. Although soils are a significant source of mercury that has been included in simulations (Gbor et al., 2006), most of the emissions are thought to be as GEM (Schroeder and Munthe, 1998). We have not included them in the inversion as the present work is focused on reactive mercury.

Emissions of GEM from the lake surface were based on a two-layer gas exchange model (Ci et al., 2011), as described in de Foy et al. (2012b). Emissions of GEM from forest fires were obtained from the Fire Inventory from NCAR (FINN) version 1 (Wiedinmyer et al., 2011), based on fire counts, land cover and vegetation data sets from MODIS combined with mercury emissions factors from Wiedinmyer and Friedli (2007). Potential impacts were simulated for 9 geographical areas as described in de Foy et al. (2012b).

To test for impacts of the free troposphere on RGM concentrations at the surface, we perform a tracer simulation with CAMx that is separate from the other simulations. All initial and boundary conditions were set to zero in the bottom 10 layers of the model (corresponding to the bottom 2 km of the atmosphere) and to 1 ng m^{-3} above. This level was chosen arbitrarily to provide a time series of surface impacts as input to the inverse model. The a posteriori estimate of tropospheric impact at the surface is obtained by multiplying the scaling factor obtained in vector x with the time series obtained from CAMx.

2.4. Chemical box model

To represent chemical formation in the inverse modeling framework, we calculate the time series of RGM that would be formed from oxidation of GEM by O_3, by the hydroxyl radical (OH) and by bromine (Br). At this stage, we only consider gas phase formation of RGM and do not include a mechanism for PHg. Because GEM concentrations are much larger than RGM, we can treat GEM as an infinite reservoir using a value of 1.25 ng m^{-3} to represent the regional background. We next calculate the reaction

rates of oxidation based on the reaction constants in Holmes et al. (2010), measured O_3 concentrations and estimated Br and OH concentrations. By using measured and estimated values of these species, we can avoid a full chemical mechanism and limit the box model to the three reactions under consideration. Br and OH are radicals that are formed in sunlight, and so we take an average estimated concentration of 0.005 ppt for Br (Holmes et al., 2010; ENVIRON, 2011) and 0.01 ppt for OH (Lawrence et al., 2001), and scale this by the normalized solar radiation. The estimated solar radiation was obtained by calculating hourly clear sky values and scaling by observations of cloud cover. To obtain a time series of RGM at the measurement site due to each pathway, we integrate the formation rate in combination with a loss rate. In reality the loss rate depends on wet and dry deposition which would require running a 3D grid model. To preserve the simplicity of the box model we use a constant loss rate corresponding to a 1 day lifetime of RGM in the atmosphere (Fain et al., 2009; Sillman et al., 2007).

3. Results & discussion

The meteorological simulations were evaluated with Integrated Surface Hourly Data at the General Mitchell International Airport (KMKE). Pearson's correlation coefficient was 0.97 for temperature, 0.95 for water vapor mixing ratio, 0.72 for wind speed and 0.74 for wind direction. Fig. 3 shows the probability density function for both the measurements and the simulations. The distributions are very similar, and all variables passed the Kolmogorov–Smirnov test to much lower than the 1% significance level, showing that the model does not suffer from significant systematic biases.

Fig. 3 also presents the autocorrelation function for the measurements and the simulations as well as for the residual between the two. This shows that errors are not significantly correlated in time beyond 12 h. For the bootstrapped simulations, we randomly select individual days rather than individual data points. In this way, we reduce the extent to which errors are correlated within our sample and hence obtain a broader range of weather conditions and a better representation of transport uncertainties in the bootstrapped samples.

The inverse model was evaluated by calculating Pearson's correlation coefficient between the reconstructed time series based on the output of the inverse model and the measurement time series, shown in Fig. 4. We excluded the data points rejected by the Iteratively Reweighted Least-Squares procedure. This yielded 0.58 for GEM, 0.65 for RGM, 0.64 for PHg and 0.65 for RHg. Annual average levels of mercury in the inverse model time series were within 10% of the average measured concentrations.

When estimating the background concentration, we use a value close to the minimum concentration in the measurements as an a priori, and let the model determine a posterior estimate. In practice, we used 1.5 ng m^{-3} for GEM and 0 pg m^{-3} for RGM, PHg and RHg as input and obtained values of 1.72 ng m^{-3} for GEM, 0.53 pg m^{-3} for RGM, 1.31 pg m^{-3} for PHg and 2.64 pg m^{-3} for RHg. The urban background of GEM is higher than the global background because it includes the impact of local sources as discussed in de Foy et al. (2012b).

The inverse gridded emissions are shown in Fig. 5 for GEM, RGM, PHg and RHg along with emissions inventories for mercury from the Toxic Release Inventory (2004) and the National Emissions Inventory (2002). For GEM, the Ohio River Valley shows up as a dominant source in all estimates and the inverse model suggests that there are underestimated sources in the southwest. The model yields an estimate of 147,000 kg $year^{-1}$ which is larger than the 46,000 kg $year^{-1}$ reported in the NEI and the 31,200 kg $year^{-1}$ reported in the TRI. The present results are also larger than the 76,000 kg $year^{-1}$ reported in de Foy et al. (2012b). The pattern of the gridded emissions has remained very similar across model configurations, but the magnitude of the inverse emissions is sensitive to the magnitude of the regularization parameters and to the value of the local background in the model. de Foy et al. (2012b) identified the underestimation of local urban sources as a reason for the discrepancy between the inverse emissions estimates and the inventories. This conclusion is further reinforced by the new results.

In contrast to GEM, reactive mercury is both formed and lost within the atmosphere on the time scale of transport within the polar grids. For GEM, the inverse results could be interpreted as providing an estimate of direct emissions. For reactive mercury

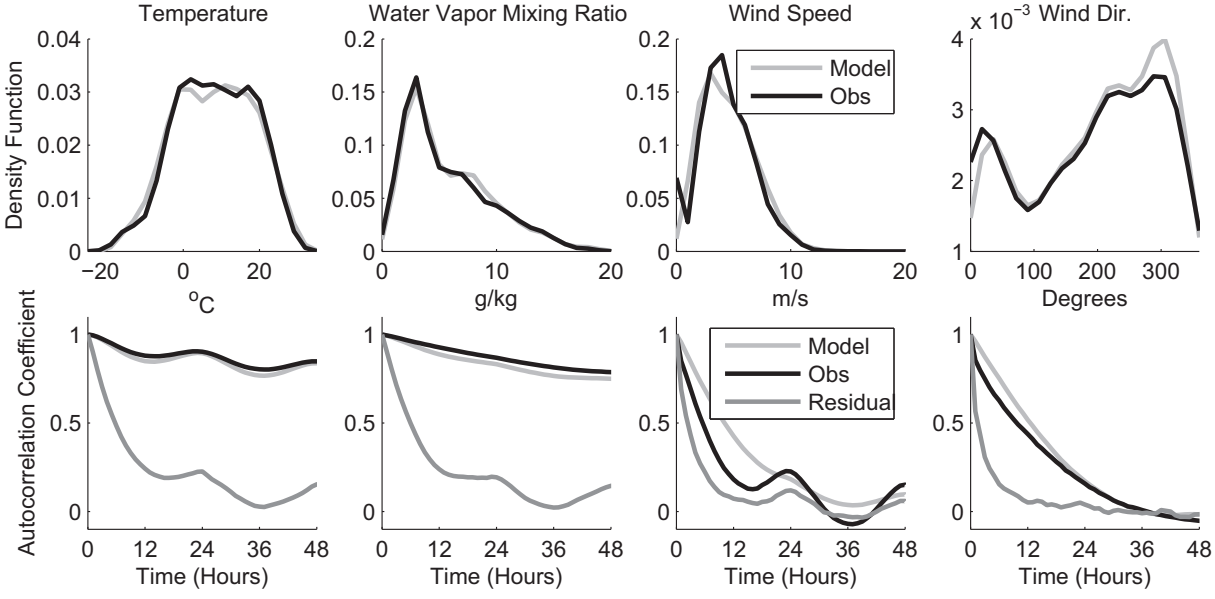

Fig. 3. Top: Probability density function of temperature, water vapor, wind speed and wind direction observations and simulations at KMKE. Bottom: Autocorrelation coefficient of observations and simulations as well as of the residual between the two.

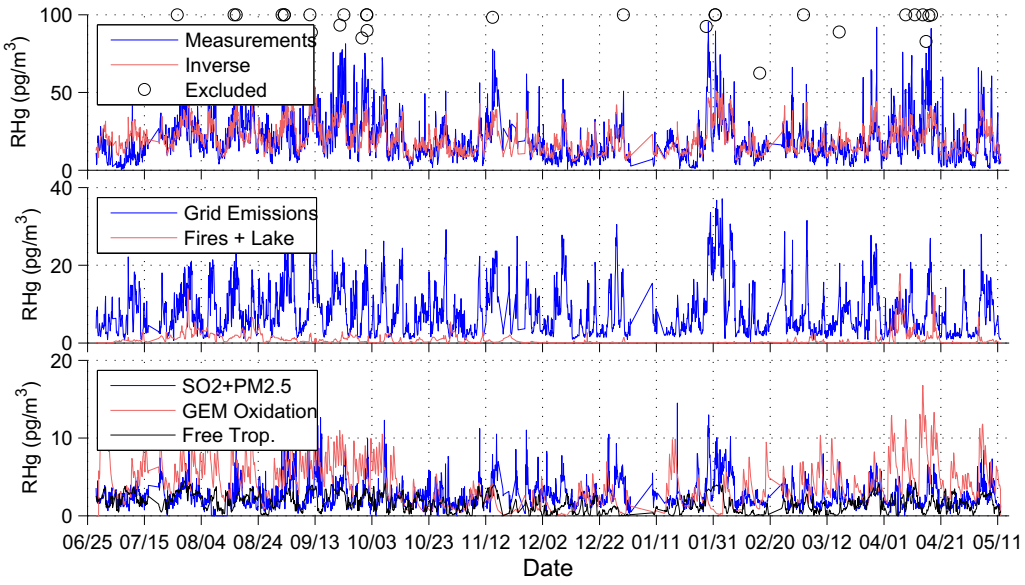

Fig. 4. Time series of RHg from the measurements and using the inverse model (top). Open circles show data points excluded by IRLS. Bottom panels show the contributions from the main source groups, including GEM oxidation calculated by the chemical box model.

however, the polar grids are an estimate of the mercury impacts which include both direct emissions and formation in the plume, but does not include mercury lost along the way. For RHg, the model estimates that Milwaukee has impacts corresponding to emissions from the Ohio River Valley as well as from the southwest. In total, the impacts at the measurement sites correspond to emissions estimates of 3000 kg year^{-1}. In addition to the two main source areas, the Chicago area stands out as a source (292 kg year^{-1}) and the region northeast of the site between the Great Lakes (505 kg year^{-1}). Although the emissions of RHg in the polar grids are much lower than GEM, they represent a significant fraction of the RHg impacts at the measurement site, as can be seen from Table 2.

For the forest fires and the lake surface emissions, the inverse model estimates a scaling factor that applies to the emissions that were used as input to the transport model. As in de Foy et al. (2012b), the model suggests that the lake emissions of GEM may be double those obtained from the parameterizations currently

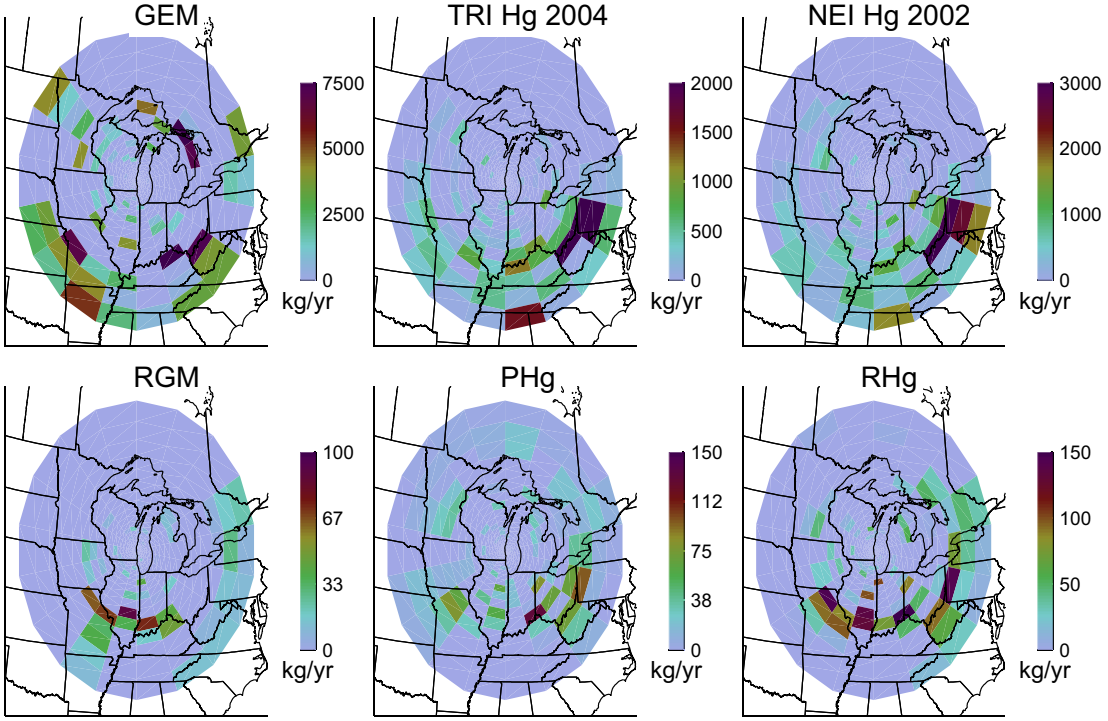

Fig. 5. Maps of gridded emissions estimated by the inverse model for GEM, RGM, PHg and RHg compared with mercury emissions from the Toxic Release Inventory (TRI) and the National Emission Inventory (NEI).

Table 1
Mean emission scaling factors determined by the inverse model for the forest fires based on GEM emissions from the FINN model and transport using CAMx. The inverse emissions of GEM are equal to the emission scaling factors multiplied by the GEM emissions in FINN. The inverse emissions of RGM, PHg and RHg are equal to the emission scaling factors multiplied by the GEM emissions in FINN divided by 100. Standard deviations are calculated based on 100 bootstrapped runs.

Hg form	Local	East	Southeast	S. Central	N. Central	West	Pacific NW	N. Canada
GEM	0.00 ± 0.03	3.73 ± 1.38	2.26 ± 1.48	1.51 ± 2.49	2.72 ± 2.11	1.25 ± 0.29	0.15 ± 0.14	0.22 ± 0.24
RGM	0.20 ± 0.17	1.26 ± 1.49	0.89 ± 1.00	0.15 ± 0.83	0.00 ± 0.59	2.33 ± 1.19	0.17 ± 0.14	0.99 ± 0.34
PHg	0.07 ± 0.16	0.00 ± 0.04	0.00 ± 0.09	0.00 ± 0.02	0.10 ± 0.08	0.00 ± 0.01	0.04 ± 0.04	0.00 ± 0.12
RHg	0.42 ± 0.48	1.62 ± 1.87	1.12 ± 1.09	0.00 ± 0.44	0.00 ± 0.82	1.09 ± 1.09	0.19 ± 0.33	0.96 ± 0.47

used. As expected, there are no significant emissions of reactive mercury from the lake.

The forest fire scaling factors are shown in Table 1. For GEM, the inverse model estimates that emissions could be up to 4 times larger than those from the FINN model for fires east of the measurement site, and that fire emissions are also underestimated for most of the other domains. The model returns a value of zero for the local domain which may be because local plumes are harder to match by the simulations than regional fire plumes, as discussed in de Foy et al. (2012b).

Emission factors of RHg are presented as a percentage of the GEM emissions in the FINN model, and are between 0.4% and 1.6% for local, east, southeast and west domains. In addition, there are estimates of 0.2% and 1.0% for the Pacific Northwest and for Northern Canada. The time series of the impacts is shown in Fig. 4. They consist mainly of RGM with minor amounts of PHg.

The forest fire emission priors have the largest uncertainty of the inputs to the model in part because of the uncertainties in the temporal profiles of the emissions, the plume injection height, and the local vegetation parameters. Overall, the inverse model suggests that GEM emissions should be increased in the FINN model, and that RHg impacts at the measurement site correspond roughly to 1% of the GEM impacts, mostly as RGM. In contrast, Finley et al. (2009) find no evidence of RGM in regional forest fire plumes measured at the Mount Bachelor Observatory in central Oregon, but do suggest that up to 15% of wildfire mercury could be emitted as PHg. Part of the discrepancy could be due to RGM formation within the plumes which is not included in the estimates by Finley et al. (2009) and PHg deposition during transport which cannot be detected by our model.

Table 2 shows the estimated fraction of each form of mercury due to different source groups (gridded emissions, CAMx simulations, AQS time series, chemical box model results and the background component). As a measure of uncertainty, we also show the standard deviations of the results calculated using bootstrapping. The histograms of bootstrapped results are shown in Fig. 6 for RHg, to show the uncertainty bounds associated with each source group. The values for RHg are in between those for RGM and PHg, as expected since RGM and PHg contribute roughly equal amounts of mercury to RHg.

Gridded emissions account for around 14% of GEM impacts at the measurement site and 41% of RHg impacts. The forest fires and lake emissions together account for 7% of GEM impacts and 4.1% of RHg impacts. Less than 1% of the GEM is coincident with the SO_2 time series, but for RHg this component increases to 2% This provides an estimate of the impact of local power plant plumes, bearing in mind that RHg is both formed and lost within the plume. The fraction of impacts coincident with $PM_{2.5}$ is estimated to be 6% for GEM and 24% for PHg.

The free troposphere is estimated to have negligible impacts on GEM, but to account for 15% of RGM. This is consistent with elevated levels of RGM aloft based on aircraft measurements off the coast of Florida (Sillman et al., 2007), as well as with measurements of mercury deposition in Nevada suggesting a free tropospheric source of RGM (Huang and Gustin, 2012).

Fig. 7 shows the simulations from the chemical box model that are input into the inverse model, and the impacts estimated by the inversion. The scaling factor on the formation of RHg by O_3 oxidation of GEM is estimated to have a value of 1 ± 0.5, suggesting that the reaction is accurately characterized. This corresponds to 4% of RHg at the measurement site being formed by this pathway (see Table 2).

The pathway through oxidation by the hydroxyl radical has a scaling factor of 37 ± 4, corresponding to 16% of the RHg. Most of the impacts are on RGM although there is a clear signal on PHg too. This suggests that this pathway is a significant source of reactive mercury that could be underestimated in the model. Because we use a proxy for the radical concentrations in the absence of measurements, there is no way to distinguish between formation due to OH, H_2O_2 and BrO. Comparing representative concentrations and the reaction rates in (Holmes et al., 2010), suggests that this pathway can be split equally between OH and H_2O_2, with only around 5% due to BrO.

Finally, the oxidation of mercury by the bromine radical is estimated to have minimal contributions to the RGM time series, but a scaling factor of 49 ± 5 for the PHg time series which corresponds to 6% of the PHg. Bromine oxidation increases with colder temperatures which leads to higher peaks in the winter, and the simulated peaks due to bromine formation match winter time PHg events (see Fig. 7). This result suggests that this pathway could be underestimated in the models, in agreement with Holmes et al. (2010, 2006) who use the reaction rates described in Goodsite et al. (2004). It is in contrast however with the new reaction rates reported by Goodsite et al. (2012); Dibble et al. (2012) which would decrease the formation of reactive mercury through bromine oxidation by a factor of 50–100.

4. Conclusions

Fig. 8 compares the source attribution of reactive mercury in this study with other published studies. In Milwaukee, our inverse model estimates that 50%–70% of RHg is associated with direct

Table 2
Impact fractions: values show the amount of mercury in the inverse time series due to each source category divided by the total amount of mercury in the inverse time series. The fraction is expressed as a percentage. The standard deviations are calculated based on 100 bootstrapped runs. Impact fractions for RGM(O_3), RGM(OH) and RGM(Br) represent the fraction of mercury due to oxidation by these three pathways. The mercury due to each reaction is calculated by multiplying the inverse scaling factor with the time series from the chemical box model.

Hg form	Gridded	CAMx	SO_2	$PM_{2.5}$	Free trop.	RGM(O_3)	RGM(OH)	RGM(Br)	Background
GEM	13.9 ± 1.9	7.2 ± 1.4	0.7 ± 0.2	5.6 ± 1.2	0.0 ± 0.7	0.2 ± 1.2	0.3 ± 0.5	0.0 ± 0.1	72.2 ± 1.8
RGM	32.2 ± 3.5	8.4 ± 3.2	2.4 ± 0.6	0.0 ± 0.0	14.8 ± 2.7	11.7 ± 3.1	24.9 ± 2.0	0.0 ± 0.0	5.7 ± 2.6
PHg	50.0 ± 3.5	0.4 ± 0.7	2.1 ± 0.6	24.0 ± 2.6	4.0 ± 1.8	0.0 ± 0.2	2.1 ± 1.9	5.7 ± 0.6	12.0 ± 1.7
RHg	40.6 ± 3.0	4.1 ± 1.8	2.3 ± 0.5	11.2 ± 2.6	8.1 ± 1.6	3.9 ± 2.1	15.5 ± 1.6	1.2 ± 0.3	13.3 ± 1.9

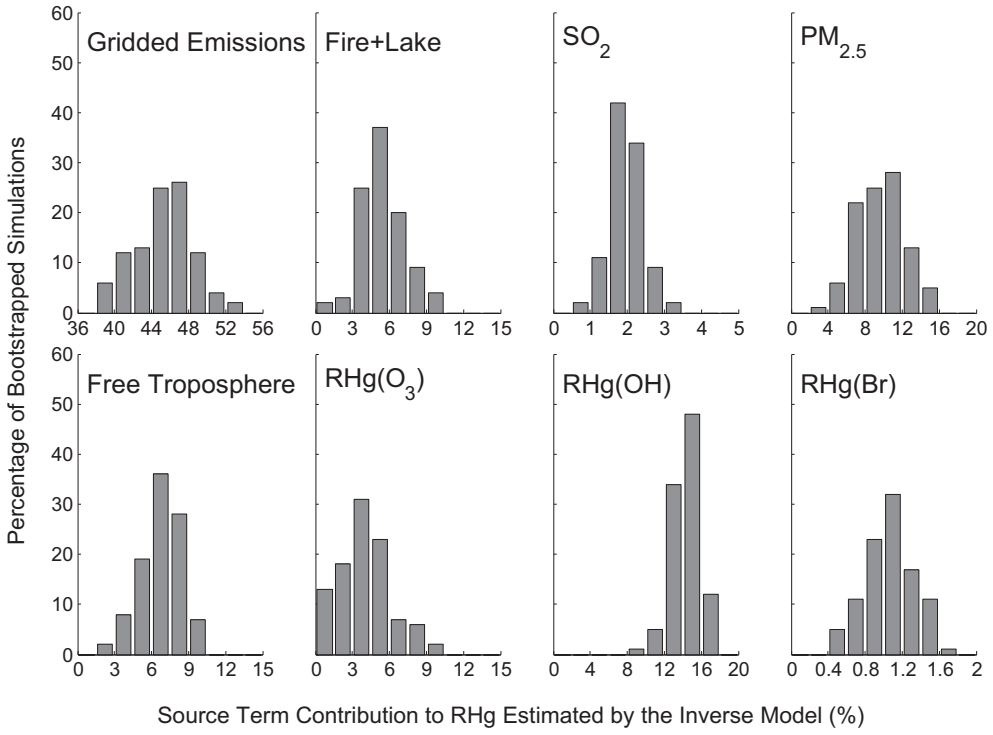

Fig. 6. Histograms showing the uncertainty of the impact fractions estimated by the inverse model for RHg. The results are based on 100 bootstrapped simulations.

emissions. For RGM, 35%–50% of the concentrations are associated with direct emissions. The inverse model was also applied to data from a rural site (Manolopoulos et al., 2007a) and results suggest that direct emissions account for 40%–65% of RHg in rural Wisconsin.

Using CMAQ-Hg and the same measurement data as this study, Holloway et al. (2012) suggest that local emissions account for 45% of reactive mercury at the urban site and only 9% at the rural site, with the balance accounted for by oxidation of global GEM. Using GEOS-Chem, Zhang et al. (2012b) find that 24% of total mercury deposition in the Midwest is due to North American anthropogenic sources, but only 14% if in-plume reduction of reactive gaseous mercury is included in the chemical mechanism. This is lower than results with CMAQ-Hg (Lin et al., 2012), which estimates that 28% of mercury deposition in the upper Midwest is due to regional sources while the remaining 72% are due to the global background. Likewise Selin and Jacob (2008) use GEOS-Chem to estimate that 30% of mercury deposition in southern Wisconsin is due to North American anthropogenic sources. Finally, a nested model suggests that 30% of the deposition is due to North American anthropogenic sources with the balance due to the rest of the world and natural sources (Seigneur et al., 2004).

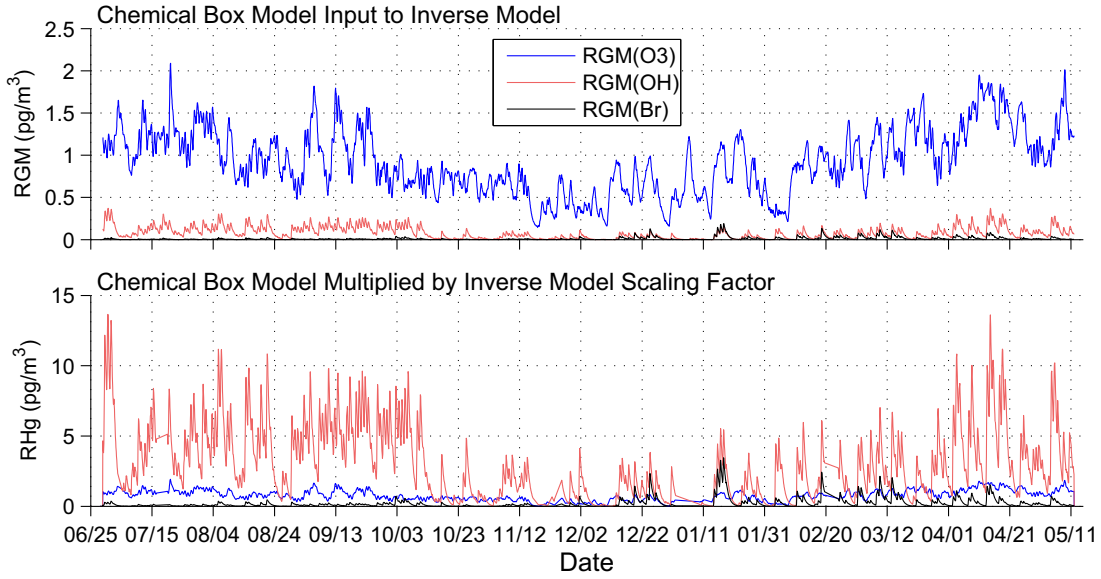

Fig. 7. Time series of chemical box model simulations for RHg formation through oxidation by ozone, the hydroxyl radical and bromine. Top: Box model simulations. Bottom: Inverse model estimates.

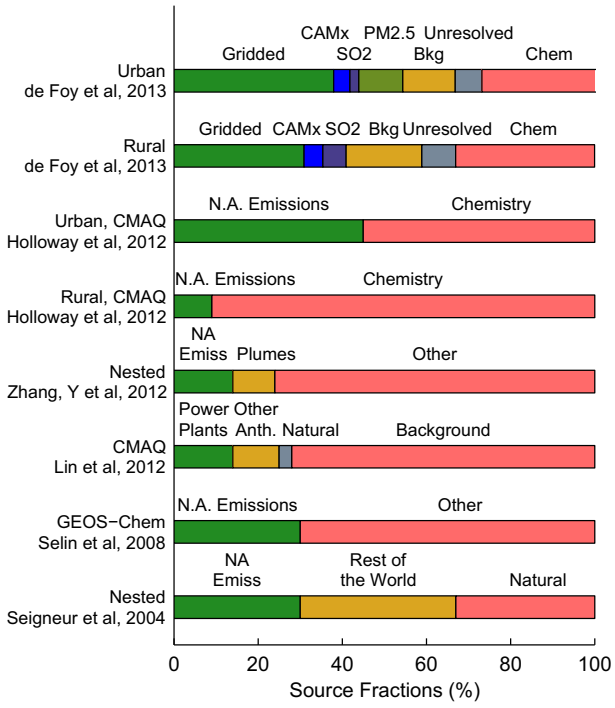

Fig. 8. Source attribution of reactive mercury using the inverse model compared with contributions to mercury deposition from the literature. NA Emissions = North American Emissions, Other Anth. = Other Anthropogenic, CAMx = Forest fires and lakes.

In conclusion, the present inverse model uses a least-squares approach to estimate the contribution of different source groups as a complementary alternative to using 3D photochemical grid models. The results provide constraints on previous estimates of mercury emissions from forest fires and from lakes, as well as formation of RGM due to atmospheric oxidation. Furthermore, they emphasize the need to develop a speciated mercury emissions inventory and to identify reasons for the underestimated emissions of GEM in current inventories. Based on measurements in urban and rural Wisconsin, the results suggest that current Eulerian models overestimate the reactive mercury formed from the global background of gaseous elemental mercury and underestimate the impacts associated with direct emissions from regional sources.

Acknowledgments

We thank C. Wiedinmyer of NCAR for the forest fire emissions. The first author would like to thank Saint Louis University for a sabbatical leave during which this research was performed, and Prof. J.-P. van Ypersele who hosted him at the Earth and Life Institute, Université catholique de Louvain. This manuscript was made possible by EPA grant number RD-83455701. Its contents are solely the responsibility of the grantee and do not necessarily represent the official views of the EPA. Further, the EPA does not endorse the purchase of any commercial products or services mentioned in the publication. The initial mercury measurements were funded by US EPA STAR Grant #R829798. We wish to thank the anonymous reviewers for their careful reviews of the paper.

References

Ashbaugh, L.L., Malm, W.C., Sadeh, W.Z., 1985. A residence time probability analysis of sulfur concentrations at grand-canyon-national-park. Atmos. Environ. 19, 1263–1270.

Aster, R.C., Borchers, B., Turber, C.H., 2012. Parameter Estimation and Inverse Problems, second ed. Academic Press.

Baker, K.R., Bash, J.O., 2012. Regional scale photochemical model evaluation of total mercury wet deposition and speciated ambient mercury. Atmos. Environ. 49, 151–162. http://dx.doi.org/10.1016/j.atmosenv.2011.12.006.

Bullock Jr., O.R., Atkinson, D., Braverman, T., Civerolo, K., Dastoor, A., Davignon, D., Ku, J.Y., Lohman, K., Myers, T.C., Park, R.J., Seigneur, C., Selin, N.E., Sistla, G., Vijayaraghavan, K., 2008. The North American Mercury Model Intercomparison Study (NAMMIS): study description and model-to-model comparisons. J. Geophys. Res. Atmos. 113. http://dx.doi.org/10.1029/2008JD009803.

Bullock Jr., O.R., Atkinson, D., Braverman, T., Civerolo, K., Dastoor, A., Davignon, D., Ku, J.Y., Lohman, K., Myers, T.C., Park, R.J., Seigneur, C., Selin, N.E., Sistla, G., Vijayaraghavan, K., 2009. An analysis of simulated wet deposition of mercury from the North American Mercury Model Intercomparison Study. J. Geophys. Res. Atmos. 114. http://dx.doi.org/10.1029/2008JD011224.

Ci, Z.J., Zhang, X.S., Wang, Z.W., Niu, Z.C., Diao, X.Y., Wang, S.W., 2011. Distribution and air-sea exchange of mercury (Hg) in the Yellow Sea. Atmos. Chem. Phys. 11, 2881–2892. http://dx.doi.org/10.5194/acp-11-2881-2011.

Dibble, T.S., Zelie, M.J., Mao, H., 2012. Thermodynamics of reactions of ClHg and BrHg radicals with atmospherically abundant free radicals. Atmos. Chem. Phys. 12, 10271–10279. http://dx.doi.org/10.5194/acp-12-10271-2012.

ENVIRON, 2011. CAMx, Comprehensive Air Quality Model with Extensions, User's Guide. Technical Report Version 5.40. ENVIRON International Corporation.

Fain, X., Obrist, D., Hallar, A.G., Mccubbin, I., Rahn, T., 2009. High levels of reactive gaseous mercury observed at a high elevation research laboratory in the Rocky Mountains. Atmos. Chem. Phys. 9, 8049–8060.

Fast, J.D., Easter, R., 2006. A Lagrangian particle dispersion model compatible with WRF. In: 7th WRF User's Workshop, Boulder, CO.

Finley, B.D., Swartzendruber, P.C., Jaffe, D.A., 2009. Particulate mercury emissions in regional wildfire plumes observed at the Mount Bachelor Observatory. Atmos. Environ. 43, 6074–6083. http://dx.doi.org/10.1016/j.atmosenv.2009.08.046.

de Foy, B., Smyth, A.M., Thompson, S.L., Gross, D.S., Olson, M.R., Sager, N., Schauer, J.J., 2012a. Sources of nickel, vanadium and black carbon in aerosols in Milwaukee. Atmos. Environ. 59, 294–301. http://dx.doi.org/10.1016/j.atmosenv.2012.06.002.

de Foy, B., Wiedinmyer, C., Schauer, J.J., 2012b. Estimation of mercury emissions from forest fires, lakes, regional and local sources using measurements in Milwaukee and an inverse method. Atmos. Chem. Phys. 12, 8993–9011. http://dx.doi.org/10.5194/acp-12-8993-2012.

Gbor, P., Wen, D., Meng, F., Yang, F., Zhang, B., Sloan, J., 2006. Improved model for mercury emission, transport and deposition. Atmos. Environ. 40, 973–983. http://dx.doi.org/10.1016/j.atmosenv.2005.10.040.

Goodsite, M., Plane, J., Skov, H., 2004. A theoretical study of the oxidation of Hg-0 to $HgBr_2$ in the troposphere. Environ. Sci. Technol. 38, 1772–1776. http://dx.doi.org/10.1021/es034680s.

Goodsite, M.E., Plane, J.M.C., Skov, H., 2012. Correction to A theoretical study of the oxidation of Hgo to $HgBr_2$ in the troposphere. Environ. Sci. Technol. 46, 5262. http://dx.doi.org/10.1021/es301201c.

Gustin, M., Jaffe, D., 2010. Reducing the uncertainty in measurement and understanding of mercury in the atmosphere. Environ. Sci. Technol. 44, 2222–2227. http://dx.doi.org/10.1021/es902736k.

Gustin, M.S., Huang, J., Miller, M.B., Peterson, C., Jaffe, D.A., Ambrose, J., Finley, B.D., Lyman, S.N., Call, K., Talbot, R., Feddersen, D., Mao, H., Lindberg, S.E., 2013. Do we understand what the mercury speciation instruments are actually measuring? Results of RAMIX. Environ. Sci. Technol. 47, 7295–7306. http://dx.doi.org/10.1021/es3039104.

Henze, D.K., Seinfeld, J.H., Shindell, D.T., 2009. Inverse modeling and mapping US air quality influences of inorganic PM(2.5) precursor emissions using the adjoint of GEOS-Chem. Atmos. Chem. Phys. 9, 5877–5903.

Holloway, T., Voigt, C., Morton, J., Spak, S.N., Rutter, A.P., Schauer, J.J., 2012. An assessment of atmospheric mercury in the Community Multiscale Air Quality (CMAQ) model at an urban site and a rural site in the Great Lakes Region of North America. Atmos. Chem. Phys. 12, 7117–7133. http://dx.doi.org/10.5194/acp-12-7117-2012.

Holmes, C.D., Jacob, D.J., Corbitt, E.S., Mao, J., Yang, X., Talbot, R., Slemr, F., 2010. Global atmospheric model for mercury including oxidation by bromine atoms. Atmos. Chem. Phys. 10, 12037–12057. http://dx.doi.org/10.5194/acp-10-12037-2010.

Holmes, C.D., Jacob, D.J., Yang, X., 2006. Global lifetime of elemental mercury against oxidation by atomic bromine in the free troposphere. Geophys. Res. Lett. 33. http://dx.doi.org/10.1029/2006GL027176.

Huang, J., Gustin, M.S., 2012. Evidence for a free troposphere source of mercury in wet deposition in the Western United States. Environ. Sci. Technol. 46, 6621–6629. http://dx.doi.org/10.1021/es3005915.

Lawrence, M., Jockel, P., von Kuhlmann, R., 2001. What does the global mean OH concentration tell us? Atmos. Chem. Phys. 1, 37–49.

Lin, C.J., Pongprueksa, P., Lindberg, S.E., Pehkonen, S.O., Byun, D., Jang, C., 2006. Scientific uncertainties in atmospheric mercury models I: model science evaluation. Atmos. Environ. 40, 2911–2928. http://dx.doi.org/10.1016/j.atmosenv.2006.01.009.

Lin, C.J., Pongprueksa, P., Russell Bullock Jr., O., Lindberg, S.E., Pehkonen, S.O., Jang, C., Braverman, T., Ho, T.C., 2007. Scientific uncertainties in atmospheric mercury models II: sensitivity analysis in the CONUS domain. Atmos. Environ. 41, 6544–6560. http://dx.doi.org/10.1016/j.atmosenv.2007.04.030.

Lin, C.J., Shetty, S.K., Pan, L., Pongprueksa, P., Jang, C., Chu, H.w, 2012. Source attribution for mercury deposition in the contiguous United States: regional difference and seasonal variation. J. Air Waste Manage. Assoc. 62, 52–63. http://dx.doi.org/10.1080/10473289.2011.622066.

Lindberg, S., Bullock, R., Ebinghaus, R., Engstrom, D., Feng, X., Fitzgerald, W., Pirrone, N., Prestbo, E., Seigneur, C., 2007. A synthesis of progress and uncertainties in attributing the sources of mercury in deposition. Ambio 36, 19–32, 8th International Conference on Mercury as a Global Pollutant, Madison, WI, AUG 06-11, 2006.

Lindberg, S., Stratton, W., 1998. Atmospheric mercury speciation: concentrations and behavior of reactive gaseous mercury in ambient air. Environ. Sci. Technol. 32, 49–57. http://dx.doi.org/10.1021/es970546u.

Lohman, K., Seigneur, C., Edgerton, E., Jansen, J., 2006. Modeling mercury in power plant plumes. Environ. Sci. Technol. 40, 3848–3854. http://dx.doi.org/10.1021/es051556v.

Manolopoulos, H., Schauer, J.J., Purcell, M.D., Rudolph, T.M., Olson, M.L., Rodger, B., Krabbenhoft, D.P., 2007a. Local and regional factors affecting atmospheric mercury speciation at a remote location. J. Environ. Eng. Sci. 6, 491–501. http://dx.doi.org/10.1139/S07-005.

Manolopoulos, H., Snyder, D.C., Schauer, J.J., Hill, J.S., Turner, J.R., Olson, M.L., Krabbenhoft, D.P., 2007b. Sources of speciated atmospheric mercury at a residential neighborhood impacted by industrial sources. Environ. Sci. Technol. 41, 5626–5633. http://dx.doi.org/10.1021/es0700348.

Mergler, D., Anderson, H.A., Chan, L.H.M., Mahaffey, K.R., Murray, M., Sakamoto, M., Stern, A.H., 2007. Methylmercury exposure and health effects in humans: a worldwide concern. Ambio 36, 3–11, 8th International Conference on Mercury as a Global Pollutant, Madison, WI, AUG 06-11, 2006.

Mesinger, F., DiMego, G., Kalnay, E., Mitchell, K., Shafran, P., Ebisuzaki, W., Jovic, D., Woollen, J., Rogers, E., Berbery, E., Ek, M., Fan, Y., Grumbine, R., Higgins, W., Li, H., Lin, Y., Manikin, G., Parrish, D., Shi, W., 2006. North American regional reanalysis. Bull. Amer. Met. Soc. 87, 343. http://dx.doi.org/10.1175/BAMS-87-3-343.

Pongprueksa, P., Lin, C.J., Lindberg, S.E., Jang, C., Braverman, T., Bullock Jr., O.R., Ho, T.C., Chu, H.W., 2008. Scientific uncertainties in atmospheric mercury models III: boundary and initial conditions, model grid resolution, and Hg(II) reduction mechanism. Atmos. Environ. 42, 1828–1845. http://dx.doi.org/10.1016/j.atmosenv.2007.11.020.

Rigby, M., Manning, A.J., Prinn, R.G., 2011. Inversion of long-lived trace gas emissions using combined Eulerian and Lagrangian chemical transport models. Atmos. Chem. Phys. 11, 9887–9898. http://dx.doi.org/10.5194/acp-11-9887-2011.

Roedenbeck, C., Gerbig, C., Trusilova, K., Heimann, M., 2009. A two-step scheme for high-resolution regional atmospheric trace gas inversions based on independent models. Atmos. Chem. Phys. 9, 5331–5342.

Rutter, A.P., Schauer, J.J., Lough, G.C., Snyder, D.C., Kolb, C.J., Von Klooster, S., Rudolf, T., Manolopoulos, H., Olson, M.L., 2008. A comparison of speciated atmospheric mercury at an urban center and an upwind rural location. J. Environ. Monitor. 10, 102–108. http://dx.doi.org/10.1039/b710247j.

Rutter, A.P., Shakya, K.M., Lehr, R., Schauer, J.J., Griffin, R.J., 2012. Oxidation of gaseous elemental mercury in the presence of secondary organic aerosols. Atmos. Environ. 59, 86–92. http://dx.doi.org/10.1016/j.atmosenv.2012.05.009.

Schroeder, W., Munthe, J., 1998. Atmospheric mercury – an overview. Atmos. Environ 32, 809–822. http://dx.doi.org/10.1016/S1352-2310(97)00293-8, 4th International Conference on Mercury as a Global Pollutant, HAMBURG, GERMANY, AUG 04–08, 1996.

Seibert, P., Frank, A., 2004. Source-receptor matrix calculation with a Lagrangian particle dispersion model in backward mode. Atmos. Chem. Phys. 4, 51–63.

Seigneur, C., Vijayaraghavan, K., Lohman, K., Karamchandani, P., Scott, C., 2004. Global source attribution for mercury deposition in the United States. Environ. Sci. Technol. 38, 555–569. http://dx.doi.org/10.1021/es034109t.

Selin, N.E., Jacob, D.J., 2008. Seasonal and spatial patterns of mercury wet deposition in the United States: constraints on the contribution from North American anthropogenic sources. Atmos. Environ. 42, 5193–5204. http://dx.doi.org/10.1016/j.atmosenv.2008.02.069.

Sillman, S., Marsik, F.J., Al-Wali, K.I., Keeler, G.J., Landis, M.S., 2007. Reactive mercury in the troposphere: model formation and results for Florida, the northeastern United States, and the Atlantic Ocean. J. Geophys. Res. Atmos. 112. http://dx.doi.org/10.1029/2006JD008227.

Skamarock, W.C., Klemp, J.B., Dudhia, J., Gill, D.O., Barker, D.M., Wang, W., Powers, J.G., 2005. A Description of the Advanced Research WRF Version 2. Technical Report NCAR/TN-468+STR. NCAR.

Stohl, A., Forster, C., Frank, A., Seibert, P., Wotawa, G., 2005. Technical note: the Lagrangian particle dispersion model FLEXPART version 6.2. Atmos. Chem. Phys. 5, 2461–2474. SRef-ID: 1680-7324/acp/2005-5-2461.

Stohl, A., Seibert, P., Arduini, J., Eckhardt, S., Fraser, P., Greally, B.R., Lunder, C., Maione, M., Muehle, J., O'Doherty, S., Prinn, R.G., Reimann, S., Saito, T., Schmidbauer, N., Simmonds, P.G., Vollmer, M.K., Weiss, R.F., Yokouchi, Y., 2009. An analytical inversion method for determining regional and global emissions of greenhouse gases: sensitivity studies and application to halocarbons. Atmos. Chem. Phys. 9, 1597–1620.

Subir, M., Ariya, P.A., Dastoor, A.P., 2011. A review of uncertainties in atmospheric modeling of mercury chemistry I. Uncertainties in existing kinetic parameters – fundamental limitations and the importance of heterogeneous chemistry. Atmos. Environ. 45, 5664–5676. http://dx.doi.org/10.1016/j.atmosenv.2011.04.046.

Subir, M., Ariya, P.A., Dastoor, A.P., 2012. A review of the sources of uncertainties in atmospheric mercury modeling II. Mercury surface and heterogeneous chemistry – a missing link. Atmos. Environ. 46, 1–10. http://dx.doi.org/10.1016/j.atmosenv.2011.07.047.

Wiedinmyer, C., Akagi, S.K., Yokelson, R.J., Emmons, L.K., Al-Saadi, J.A., Orlando, J.J., Soja, A.J., 2011. The Fire INventory from NCAR (FINN): a high resolution global model to estimate the emissions from open burning. Geosci. Model Dev. 4, 625–641. http://dx.doi.org/10.5194/gmd-4-625-2011.

Wiedinmyer, C., Friedli, H., 2007. Mercury emission estimates from fires: an initial inventory for the United States. Environ. Sci. Technol. 41, 8092–8098. http://dx.doi.org/10.1021/es071289o.

Wunsch, C., 2006. Discrete Inverse and State Estimation Problems: With Geophysical Fluid Applications. Cambridge University Press.

Zhang, L., Blanchard, P., Gay, D.A., Prestbo, E.M., Risch, M.R., Johnson, D., Narayan, J., Zsolway, R., Holsen, T.M., Miller, E.K., Castro, M.S., Graydon, J.A., St Louis, V.L., Dalziel, J., 2012a. Estimation of speciated and total mercury dry deposition at monitoring locations in eastern and central North America. Atmos. Chem. Phys. 12, 4327–4340. http://dx.doi.org/10.5194/acp-12-4327-2012.

Zhang, Y., Jaegle, L., van Donkelaar, A., Martin, R.V., Holmes, C.D., Amos, H.M., Wang, Q., Talbot, R., Artz, R., Brooks, S., Luke, W., Holsen, T.M., Felton, D., Miller, E.K., Perry, K.D., Schmeltz, D., Steffen, A., Tordon, R., Weiss-Penzias, P., Zsolway, R., 2012b. Nested-grid simulation of mercury over North America. Atmos. Chem. Phys. 12, 6095–6111. http://dx.doi.org/10.5194/acp-12-6095-2012.